Supplementary Information

CeF_3/Co_3O_4 Heterojunction Enabled Reconstruction Regulation for Selective and Efficient Electrocatalytic Cleavage of Lignin C_β–O–4 linkage

Jialin Fan[a], Jingxuan Zhang[a], Wenjing Bai[a], Zhaoling Ma[b], Liyuan Gong[a,*], Yongzhuang Liu[a,*], Shuo Dou[a,*]

[a]*State Key Laboratory of Utilization of Woody Oil Resource, Key Laboratory of Bio-Based Material Science and Technology of Ministry of Education, Northeast Forestry University, Hexing Road 26, Harbin, 150040, China*

E-mail: doushuo@nefu.edu.cn; lyz@nefu.edu.cn; gly@nefu.edu.cn

[b]*Guangxi Key Laboratory of Low Carbon Energy Materials, Guangxi Normal University, Guilin, 541004, China*

Experimental section

1. Catalysts preparation and characterization

Material. Except noted, all chemicals were purchased and used without further purification. Deionized water was used throughout the experiments. Cobalt (II) nitrate hexahydrate ($Co(NO_3)_2·6H_2O$, A.R.), cerium nitrate hexahydrate ($Ce(NO_3)_3·6H_2O$, A.R.), urea (CH_4N_2O, A.R.), ammonium fluoride (NH_4F, AR), hydrochloric acid (HCl, 36.0%–38.0%), ethanol (C_2H_6O, A.R.), 2-phenoxyacetophenone (PP–one, 98%), ammonium chloride (NH_4Cl, A.R.) were purchased from Beijing InnoChem Science & Technology Co., Ltd. (China).

Preparation of bulk Co_3O_4 and CeF_3/Co_3O_4. Nickel foam (NF) was used as matrix for growing Co_3O_4 nanoneedle arrays. Before the hydrothermal process, NF (30 × 30 × 2 mm) was ultrasonically cleaned by HCl, ethanol, and deionized water for 15 min to get rid of the possible surface dirt and oxide layer. Typically, $Co(NO_3)_2·6H_2O$ (6 mmol), urea (30 mmol), and NH_4F(0.2 g) were dissolved in deionized water (60 mL) under stirring to form a homogeneous solution. Then, the mixed solution with a clean NF was transformed into a Teflon-lined stainless-steel autoclave and maintained at 120 ^oC for 10 h. After cooling to room temperature, the substrate was taken out and cleaned with deionized water and ethanol several times before being fully dried at 60 ^oC. After annealing at 400 ^oC for 2h under air atmosphere, Co_3O_4 was obtained. CeF_3/Co_3O_4 were prepared by replacing 20% molar ration of $Co(NO_3)_2·6H_2O$ with $Ce(NO_3)_3·6H_2O$ under the same procedure.

Characterizations. The sample morphologies were characterized by SEM (ZEISS Sigma 360, Germany) and TEM (JEOL JEM–2100F, Japan). X-ray diffraction (XRD) was conducted in the 2θ range of 10−80° at a scan rate of 5 ^{o}/min with Cu–Kα radiation (Rigaku Ultima IV, Japan). The X-ray photoelectron spectroscopy (XPS) was performed by Thermo Scientific K-Alpha (USA). Raman and in-situ Raman spectra were measured on a confocal microscope (Renishaw, England) equipped with a semiconductor laser (λ=785 nm). Qualitative and quantitative analysis for lignin model cleavage products and lignin depolymerization products were carried out on gas chromatography-mass spectrometry (GC-MS, Agilent 7890A -5975C, HP-5MS column, USA) and gas chromatography (GC, Agilent 8860, HP-5 column, USA), respectively. Organosolv lignin, pre-oxidized lignin, and depolymerization product fractions were

characterized by HSQC NMR (Bruker Advance III HD 500 MHz, Switzerland). Gel permeation chromatography (GPC) of pre-oxidized lignin and depolymerization product fractions was conducted using THF as the mobile phase on a Waters 1525.

Electrochemical measurements. All electrochemical measurements were performed on an electrochemical workstation (CHI 660 E), and the performance of electrocatalysts was evaluated in a single cell by using a typical three-electrode system. In such a system, mixed electrolyte (2.5 mL ethanol, THF, and 5mL 1M KOH) was employed, Pt foil and Ag/AgCl served as the counter and reference electrode. The LSV measurement was performed at a scan rate of 5 mV/s, and the potential in the LSV polarization curves was corrected by iR compensation at the level of 90%. EIS tests were conducted from 0.1 Hz to 100000Hz, and the results are presented in the form of a Bode phase plot.

2. Synthesis of Lignin β–O–4 Model Compounds

β–O–4 ketone models were prepared following previously reported procedures.[1] The substrates utilized in this work were synthesized via two steps from the corresponding phenolic compounds (phenol, guaiacol, 2,6-dimethoxyphenol) and bromoacetophenone derivatives (2-bromoacetophenone, 4-methoxy–α–bromoacetophenone, bromo-3,4-dimethoxyacetophenone). First, the bromoacetophenone derivatives (5 mmol) were added to potassium carbonate (7.5 mmol) in 50 mL of acetone, followed by the slow dropwise addition of the phenolic compounds (6.25 mmol), also dissolved in 50 mL of acetone. The resulting mixture was stirred at reflux for 5 h, then filtered through diatomaceous earth under vacuum and concentrated by rotary evaporation. The residue was dissolved in 20 mL of ethanol and recrystallized to afford white or yellowish crystals.

3. Preparation of pre-oxidized poplar lignin

Extraction of lignin. Prior to extraction, wood powder was crushed to increase its surface area, thereby enhancing extraction efficiency. The extraction process was carried out in a Soxhlet apparatus. The extraction solution consisted of 400 mL of 1,4–dioxane, 0.9 mL of hydrochloric acid, and 10 mL of deionized water and was heated to boiling point until it became clear and transparent. The mixed solution was then cooled to room temperature and concentrated by rotary evaporation. Subsequently, the concentrate was added to deionized water with an appropriate amount of NH_4Cl. Finally, poplar lignin was obtained by filtration and drying at

room temperature.

DDQ pre-oxidized lignin. 0.5 g of poplar lignin and 0.15 g of 2,3–dicyano–5,6–dicyano–1,4–benzoquinone were dissolved in 20 mL of 1,4–dioxane. After O_2 has been circulated for 10 minutes, O_2 was pumped into a high-pressure reactor to maintain a pressure of 1 MPa. The oxidation reaction was conducted at 90 °C for 2 h with stirring at 400 rpm. Next, the mixed solution was cooled to room temperature and concentrated by rotary evaporation. The concentrate was then added to deionized water. Finally, pre–oxidized poplar lignin was obtained by filtration and drying at room temperature.

Calculation of products from lignin model and lignin material cleavage.

Lignin models:

$$\text{Yield of product monomer} = \frac{\text{mole of monomer}}{\text{mole of lignin model}} \times 100\%$$

$$\text{Conversion of lignin model} = \left(1 - \frac{\text{mole of residual lignin model}}{\text{mole of lignin model}}\right) \times 100\%$$

Pre-oxidized poplar lignin:

$$\text{Yield of product monomer (wt\%)} = \frac{\text{mole of monomer} \times M}{\text{mass of lignin}} \times 100\%$$

M: Molecular weight of monomer

The mole of every product was calculated by the external standard method of GC.

Figures and Tables

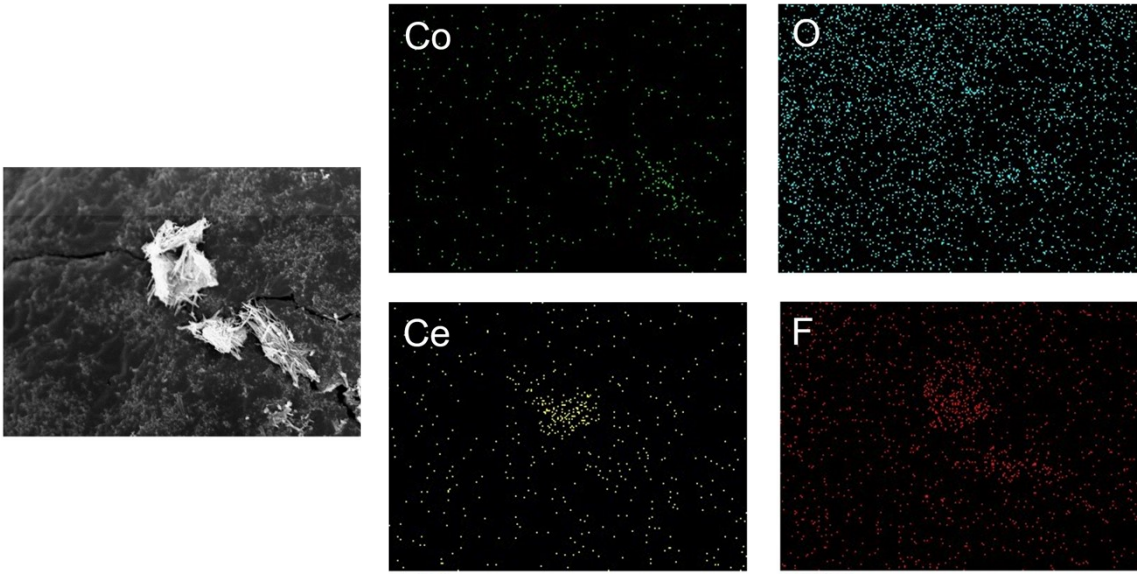

Fig. S1. Element mapping images of CeF_3/Co_3O_4.

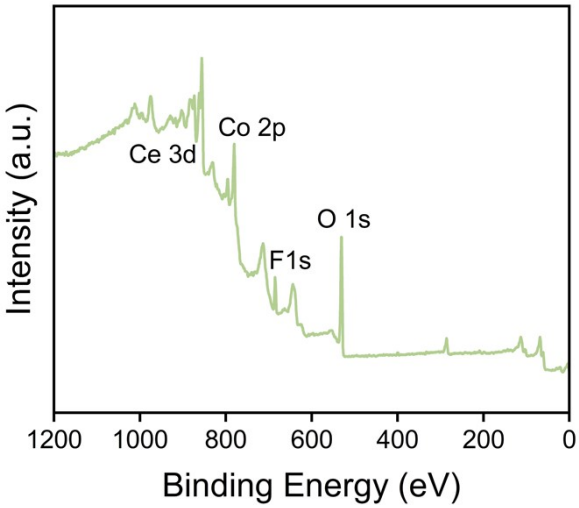

Fig. S2. XPS survey spectra of CeF_3/Co_3O_4.

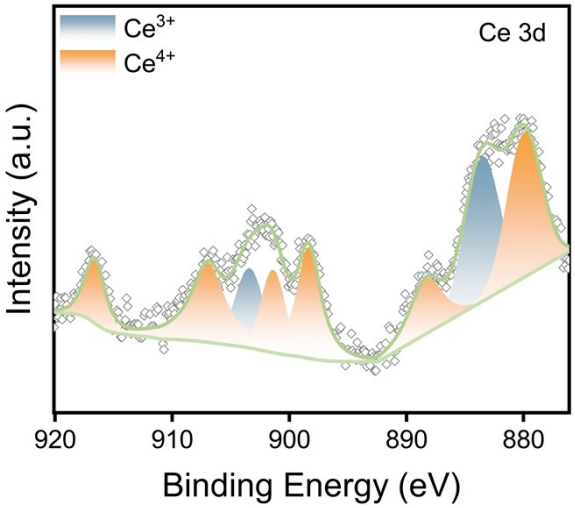

Fig. S3. Ce 3d spectra of CeF_3/Co_3O_4.

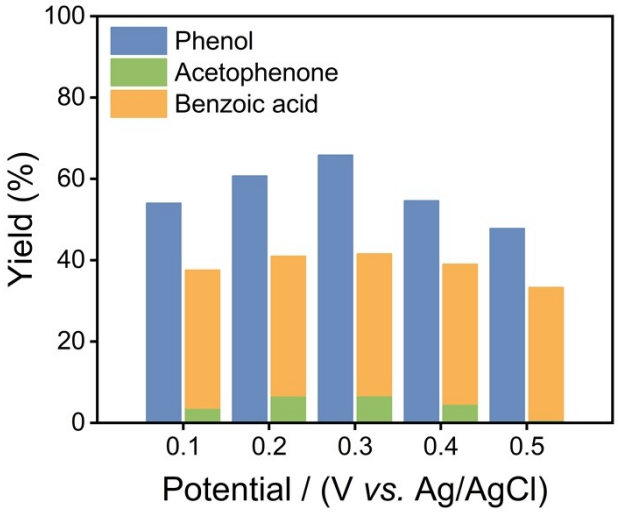

Fig. S4. The yield of products of Co_3O_4 under different potentials.

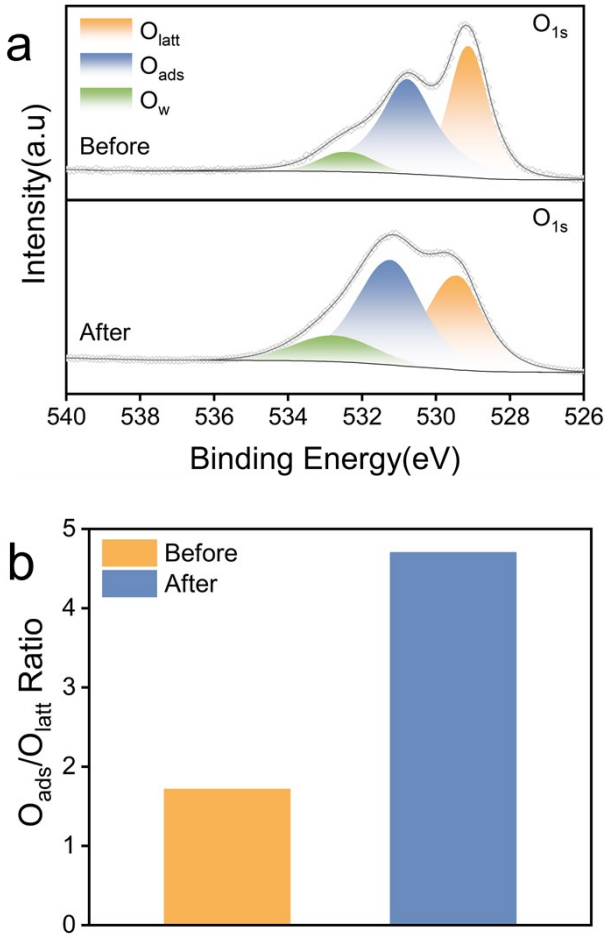

Fig. S5 (a) O 1s of CeF_3/Co_3O_4 before and after reaction. (b) The ratio of O_{ads}/O_{latt} before and after reaction.

The transformation from Co_3O_4 to CoOOH is driven by the rapid accumulation of surface OH* species.[2, 3] During alkaline oxygen evolution reaction (OER), Co_3O_4 undergoes an amorphous $Co(OH)_6$ intermediate state.[4] Owing to the kinetic mismatch between fast OH* adsorption and relatively slow deprotonation, the surface coordination structure is further disrupted. [5, 6] Further investigation reveals that surface OH* perturbs the charge distribution equilibrium among different cobalt valence states, thereby driving surface reconstruction of the cobalt-based material.[7]

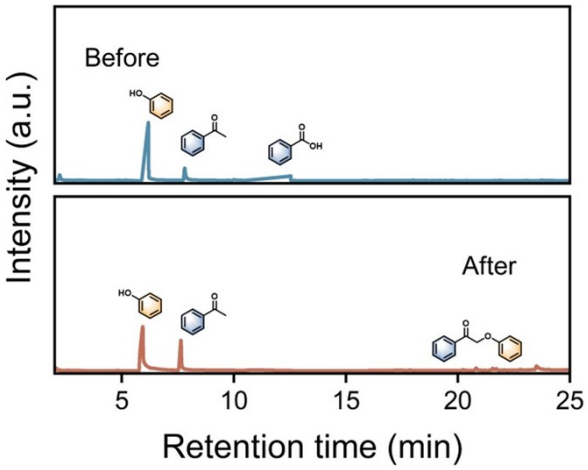

Fig. S6. GC of electrocatalytic oxidative reaction solution on CeF_3/Co_3O_4 catalyst with L-Ascorbic acid under standard reaction conditions.

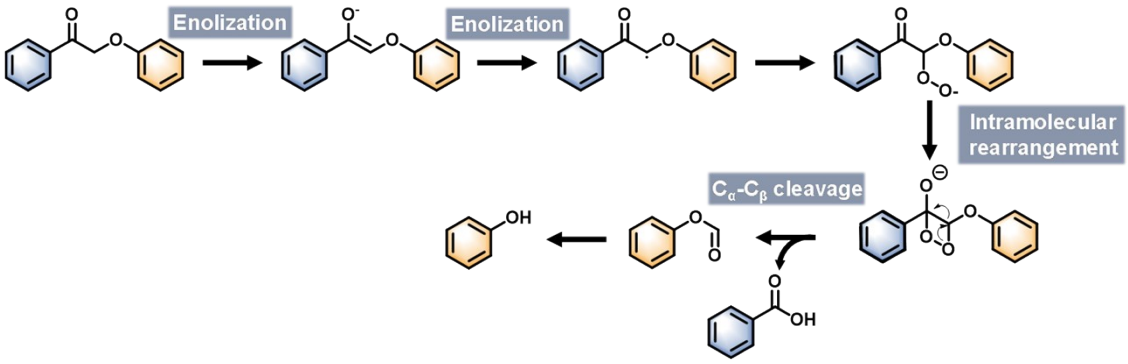

Fig. S7. Main reaction pathway of C_α–C_β bond cleavage in the PP-one.

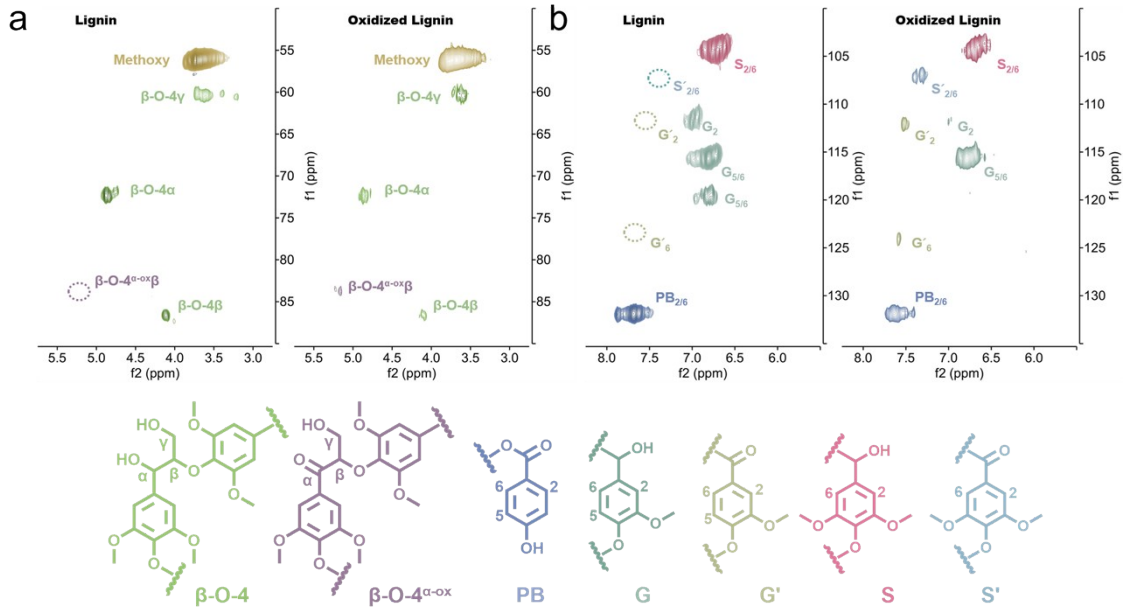

Fig. S8. 2D HSQC NMR spectra of poplar lignin before and after oxidation.

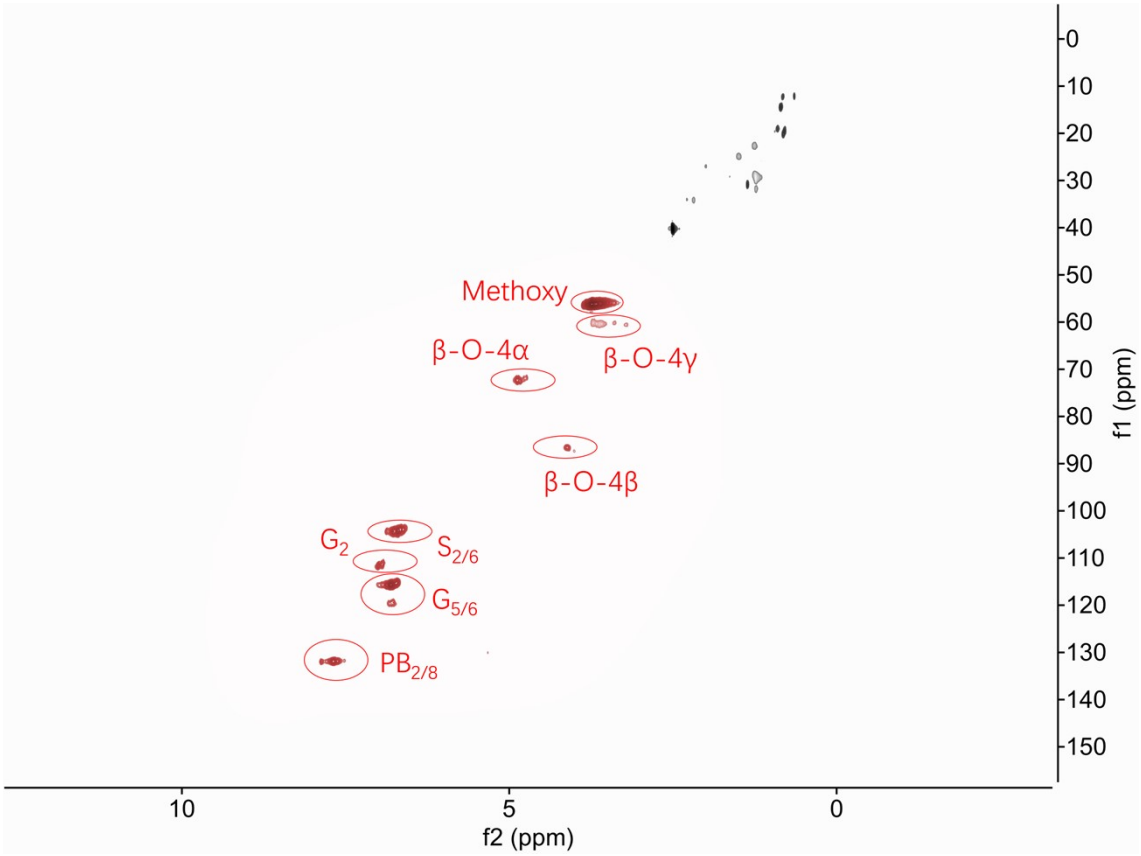

Fig. S9 The raw 2D HSQC NMR spectrum of poplar lignin before oxidation

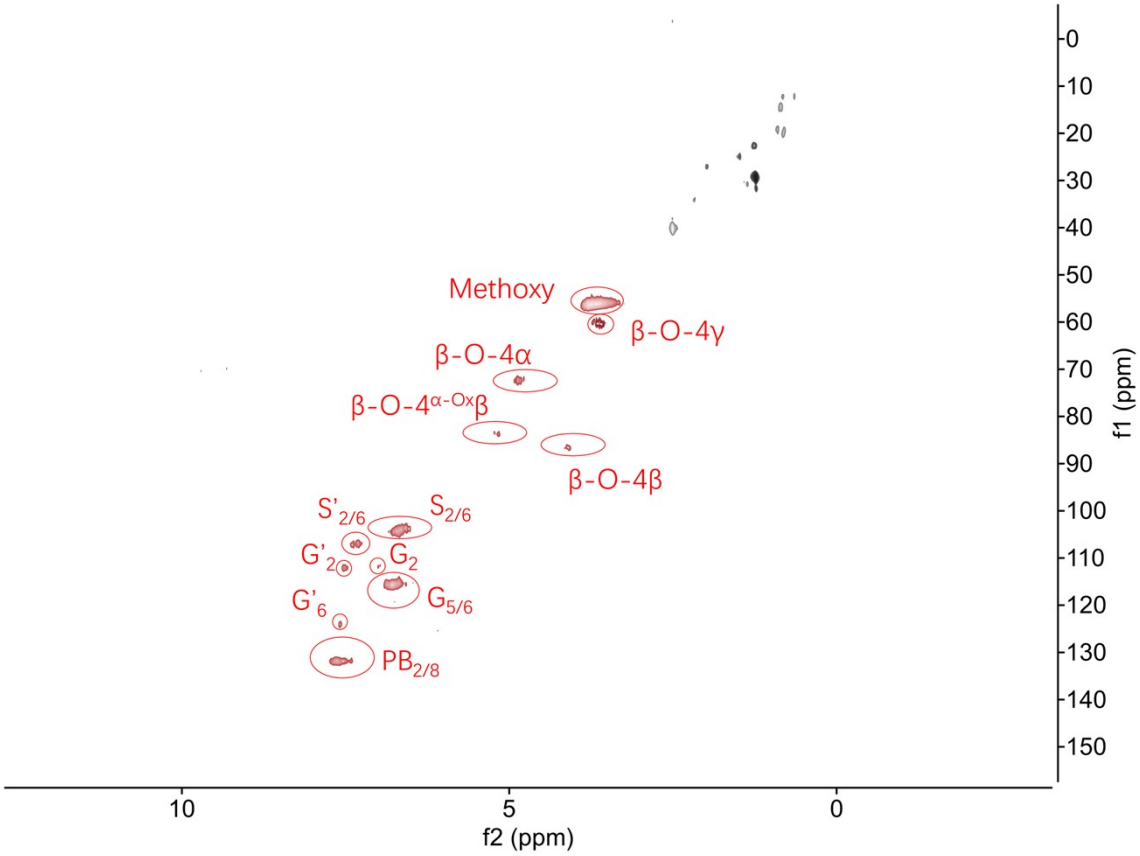

Fig. S10 The raw 2D HSQC NMR spectrum of poplar lignin after oxidation

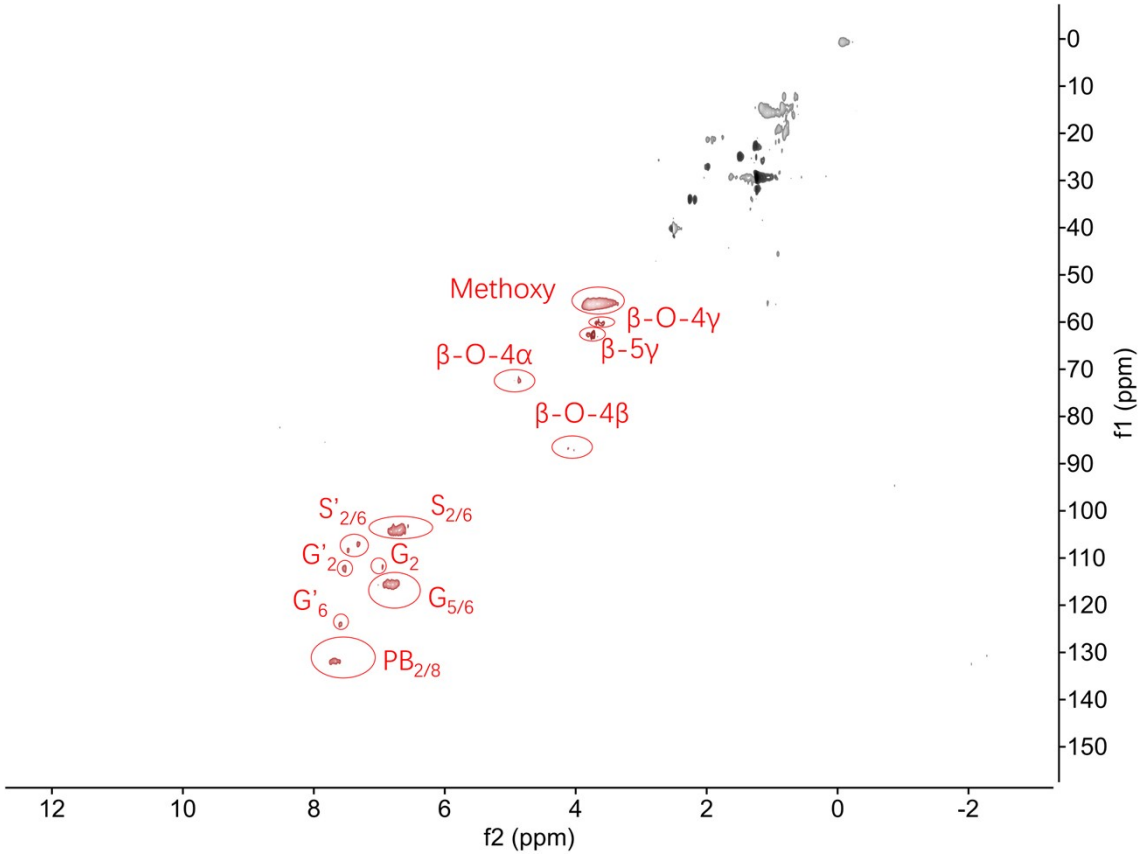

Fig. S11 The raw 2D HSQC NMR spectrum of poplar lignin after electrocatalytic reaction.

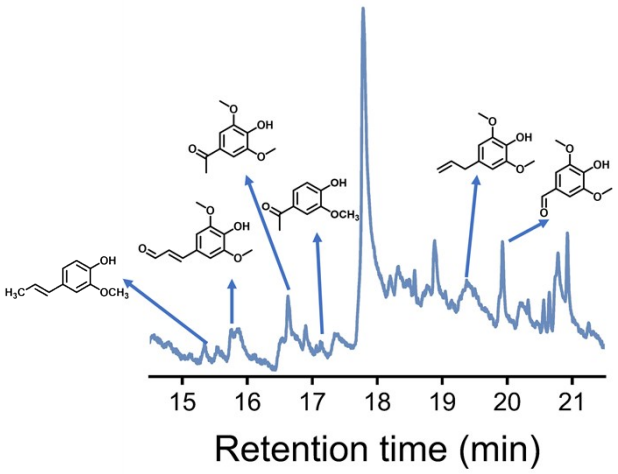

Fig. S12. GC–MS chromatograms of the electrocatalytic depolymerization of poplar lignin.

Table S1. Comparison of C_β–O–4 bond cleavage efficiency from 2-phenoxyacetophenone on CeF_3/Co_3O_4 with other catalysts.

Catalyst	Reaction conditions	Con. (%)	Yield of phenol	Yield of C–C bond cleavage products	Yield of C–O bond cleavage products	Refs
CeF_3/Co_3O_4	**0.3 V vs. Ag/AgCl, RT**	**≥99**	**91.21 %**	**Benzoic acid 44.66%**	**Acetophenone 11.97%**	**This work**
d–CNTs	0.5 V vs. Ag/AgCl, RT	98.79	62.31 %	Benzoic acid 43.42%	none	Ref.[8]
Pd/CeO_2	50°C	94.60	87.4%	Benzoic acid 84.5%	none	Ref.[9]
CTFs	140°C, 0.5 MPa O_2	＞99	56%	Benzoic acid 4%, Methyl benzoylformate 18%	Methyl benzoate 10%,	Ref.[10]
NiCo-AB MOF	0.34 V vs. Ag/AgCl , RT	97	76.3%	none	Acetophenone 21.7%	Ref.[11]
CTF-Pdcb-1	160°C, 0.5 MPa O_2	＞99	45.1%	Benzoic acid 24%, Methyl benzoylformate 8%	Methyl benzoate 14.9%,	Ref.[12]

Table S2. C_β–O–4 cleavage range of typical lignin models

Entry	Substrate Conversion (%)	Yield of benzoic acid (%)	Yield of phenol (%)	Entry	Substrate Conversion (%)	Yield of benzoic acid (%)	Yield of phenol (%)
1	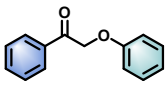	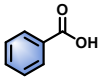		**6**	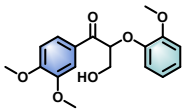	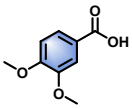	
	≥99	44.66	91.21		99.18	19.91	22.31
2	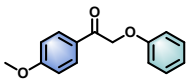	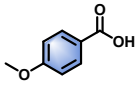		**7**	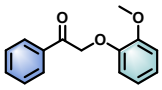	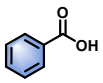	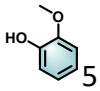
	98.13	29.91	69.23		≥99	32.27	0.4
3	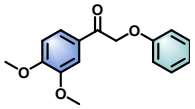	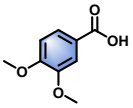		**8**	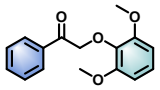		
	91.65	13.03	63.43		96.5	27.46	46.1
4	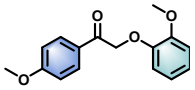	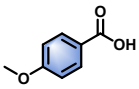		**9**	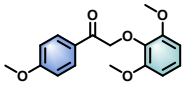	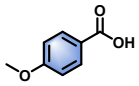	
	98.3	19.29	56.62		99.41	11.98	17.12
5	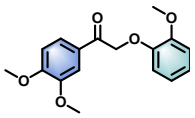	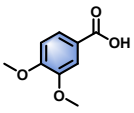		**10**	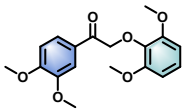	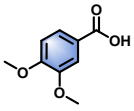	
	97.69	10.85	39.91		99.29	10.85	17.71

Table S3. Comparison of lignin depolymerization performance: our system vs. conventional electrocatalytic systems.

Catalyst	Reaction conditions	Yield of monomeric product	Refs
CeF_3/Co_3O_4	**0.3 V vs. Ag/AgCl, RT**	**15.02 wt%**	**This work**
Pt	TBHP, 20 mA/cm^2, RT	5 wt%	Ref.[13]
d-CNTs	0.5 V vs. Ag/AgCl, RT	12.41 wt%	Ref.[8]
Mo@NiOOH	TBHP,3.5V vs. Ag/AgCl, RT	13 wt%	Ref.[14]
NiCo-AB MOF	0.34 V vs. Ag/AgCl, RT	12.48wt%	Ref.[11]
Ni $(OH)_2$–V	1.4 V_{RHE}, RT	14.24 wt%	Ref.[15]
Au/CuO	1.0V_{RHE}, 40 ^oC	10.8 wt%	Ref.[16]
Pb/PbO_2	30 mA/cm^2	3.6 wt%	Ref.[17]
Ni	12.5 mA/cm^2, 160 ^oC	4.2 wt%	Ref.[18]

References

1 J. Li, Z. Li, J. Dong, R. Fang, Y. Chi and C. Hu, ACS Catal, 2023, 13, 5272-5284.
2 Y. Li, L. Yin, J. Liu, X. Qin, X. Lu, X. Dai, K. Qi, Y. Yang, W. Qi and G. Liu, Nat Sustainability, 2025, 8, 1524-1532.
3 W. Hu, J. Zhang, Y. Fan, C. Zhao, H. Wang, J. Du, Y. Fang, C. Li, C. Cao, Y. Li, A. Li, Z. Li and C. Li, J Am Chem Soc, 2026, 148, 16267-16277.
4 R. Zhang, L. Pan, B. Guo, Z.-F. Huang, Z. Chen, L. Wang, X. Zhang, Z. Guo, W. Xu, K. P. Loh and J.-J. Zou, J Am Chem Soc, 2023, 145, 2271-2281.
5 Z. Xiao, Y.-C. Huang, C.-L. Dong, C. Xie, Z. Liu, S. Du, W. Chen, D. Yan, L. Tao, Z. Shu, G. Zhang, H. Duan, Y. Wang, Y. Zou, R. Chen and S. Wang, J Am Chem Soc, 2020, 142, 12087-12095.
6 H. B. Tao, Y. Xu, X. Huang, J. Chen, L. Pei, J. Zhang, J. G. Chen and B. Liu, Joule, 2019, 3, 1498-1509.
7 M. Cui, R. Guo, Y. Zhou, W. Zhao, Y. Liu, W. Luo, Q. Ou and S. Zhang, ACS Catal, 2024, 14, 16353-16362.
8 J. Zhang, W. Bai, J. Xu, A. Zhou, J. Fan, J. Bi, Q. Zhou, L. Gong, Y. Liu, S. Dou, H. Yu and S. Wang, Angew Chem Int Ed, 2025, 64, e202510437.
9 Y. Hu, Y. Cui, S. Zhao, X. Zhao, X. Hu, Z. Song, W. Fan and Q. Zhang, Green Chem, 2023, 25, 5150-5159.
10 G. Zhu, S. Shi, L. Zhao, M. Liu, J. Gao and J. Xu, ACS Catal, 2020, 10, 7526-7534.
11 W. Bai, X. Wang, J. Xu, Y. Liu, Y. Lou, X. Sun, A. Zhou, H. Li, G. Fu, S. Dou and H. Yu, Adv Sci, 2024, 11, 2403431.
12 L. Zhao, S. Shi, M. Liu, G. Zhu, M. Wang, W. Du, J. Gao and J. Xu, Green Chem, 2018, 20, 1270-1279.
13 L. Ma, H. Zhou, X. Kong, Z. Li and H. Duan, ACS Sustainable Chem Eng, 2021, 9, 1932-1940.
14 J. Xu, J. Meng, Y. Hu, Y. Liu, Y. Lou, W. Bai, S. Dou, H. Yu and S. Wang, Research, 2023, 6, 0288.
15 Y. Yang, L. Kong, Z. Xia, Y. He, Y. Li, S. Wang and Y. Zou, J Am Chem Soc, 2025, 147, 35924-35934.
16 C. Wang, Q. Luo, L. Xu, Z. Xia, Y. Zou, Y. Yang, Y. He, S. Wang and Y. Zou, Adv Mater, 2025, 37, e08234.
17 C. Lan, H. Fan, Y. Shang, D. Shen and G. Li, Sustainable Energy Fuels, 2020, 4, 1828-1836.
18 M. Zirbes, L. L. Quadri, M. Breiner, A. Stenglein, A. Bomm, W. Schade and S. R. Waldvogel, ACS Sustainable Chem Eng, 2020, 8, 7300-7307.